IEEE Access
Multidisciplinary | Rapid Review | Open Access Journal

Received April 12, 2021, accepted May 20, 2021, date of publication May 25, 2021, date of current version June 3, 2021.

Digital Object Identifier 10.1109/ACCESS.2021.3083506

Optimal Design of High-Speed Double-Sided Linear Permanent Magnet Motors With Segmented Trapezoidal Magnetic Poles

DUNHUANG XU, DONG WANG, AND MING YAN

National Key Laboratory of Science and Technology on Vessel Integrated Power System, Naval University of Engineering, Wuhan 430033, China

Corresponding author: Ming Yan (hustym@sohu.com)

This work was supported by the National Science Foundation of China under Grant 51825703 and Grant 51690181.

ABSTRACT For the kilometer-level electromagnetic launch system, a high-speed double-sided linear permanent magnet (PM) linear motor is presented in this paper. To enhance the average thrust force, reduce the thrust ripple and normal force of linear motor, a segmented trapezoidal PM shaping method is proposed. Compared with conventional PM shaping method, the segmented trapezoidal PMs achieves less force ripple, greater average force and lower manufacturing difficulty. The risk of PM demagnetization fault has been taken into account. To reduce the losses in the mover of the linear motor, a non-metallic light-weight mover structure is proposed. The effectiveness of segmented trapezoidal PMs and non-metallic light-weight mover are verified by the finite element method and experiment.

INDEX TERMS Electromagnetic launch system, permanent magnet linear motors, permanent magnetic shaping method, optimal design.

I. INTRODUCTION

The electromagnetic launch system (EMLS) is a revolutionary launch system, which can accelerate the target objects to high speed in a short distance. Compared with the traditional launch systems based on the mechanical energy or chemical energy, the EMLS has certain features such as high power, high efficiency, high reliability and great dynamic performance [1], [2]. The double-sided linear permanent magnet motor (LPMM) for electromagnetic aircraft launcher was first presented in 2002 [3]. And the double-sided linear induction motor (LIM) for EMLS was presented in 2004. Due to the simple structure of secondary and high thrust density, the LIM is adopted in practical finally. With the development of technology, the EMLS can be applied more comprehensively. In this paper, a double-sided LPPM is designed for a high-speed kilometer-level EMLS. The target of the EMLS is to accelerate the object to more than 800 km/h in 500 meters and stop the object in another 500 meters.

Due to the high thrust density demand, the double-sided linear motors are more suitable than single-side motors for the EMLS. The double-sided motors can be classified into double-movers type and interior-mover type. The Double-movers long-primary LPPM is proposed in [4]. However, the yoke core of the secondary increases the mass of the movers. On the other hand, the double-sided linear motor can also be classified into the long primary type and the long secondary type. Due to the high price of the PMs, the LPMM with long secondary [5], [6] are too expensive to be used as the propulsion motors in the kilometer-level EMLS.

In recent years, the linear flux-switching PM motor (LFSPMM) have attracted widely attention [7], [8]. However, two shortages of the LFSPMM limit its application for the kilometer-level EMLS. First, the PMs are located in the primaries which makes the price of the long-primary LFSPMM unacceptable. Second, the frequency of the armature current in LFSPMM is several times higher than that of the LPMM with the same slot pitch, which limit the speed of the LFSPMM [9]. Therefore, the double-sided long-primary LSM with interior secondary is still the main topology of the EMLS.

In summary, the double-sided long-primary LPPM and LIM are two suitable topology structures for the kilometer-level high-speed EMLS. The simple comparative analysis between the LPPM and LIM is present in this paper, and the paper focus on the LPPM, finally. The main electromagnetic performance of double-sided LPPM has been discussed

The associate editor coordinating the review of this manuscript and approving it for publication was Sonia F. Pinto.

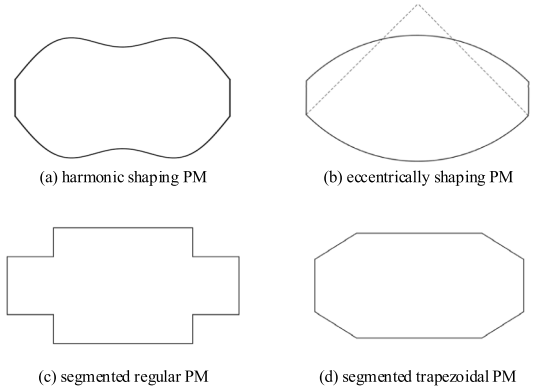

FIGURE 1. Several PM shaping methods.

TABLE 1. Design Requirements and Constraints of Linear Motors.

Items	Value
Maximum velocity	222 m/s
Maximum thrust force	80 kN
Acceleration distance	500 m
Braking distance	500 m
Pole pitch	> 400 mm
One-side air-gap	> 10 mm
Number of phase	3
Rated phase current	< 6000 Arms
Peak phase voltage	< 5000 V
Mover mass	< 250 kg

in [10], [11]. In this paper, a new PM shaping method is proposed to optimize thrust characteristics of double-sided LPPM.

For the double-sided linear PM motors with coreless secondary, the PM shaping method is one of the simplest and most effective methods to reduce the force ripple. On one hand, the average thrust force of the motor is positive correlation with the fundamental air gap flux density, and the force ripple is positive correlation with the harmonic component of the air gap flux density. On the other hand, under given air-gap space constraint, the harmonic component can enhance the fundamental component of the air-gap flux density. To increase the average force and decrease the force ripple, a PM shaping method utilizing the third harmonic was proposed in [12]. The optimal design of the shaping PM poles with third harmonic is presented in [13], as shown in Fig. 1(a). The shaping PM poles with higher order harmonic are present in [14]. However, due to the leakage flux of the PM field, the air gap flux distribution in the motors with sinusoidal and third harmonic shaping PM poles still has non-negligible high-order harmonic.

To simplify the PM structure, the traditional shaping methods always are determined by 1-2 design variables [15], [16]. For the eccentrically shaping PM, the design variables are radius of the PM surface curvatures and pole arc coefficient, as shown in Fig. 1(b). The shaping PMs also can be simplified as several regular segment with different width [17] and height [6], [18], as shown in Fig. 1(c). The trapezoidal PM poles are presented in [19]. However, the simplified structure of the traditional PM shaping methods limit their search space. Thus, a new PM shaping method is proposed in this paper, which can be called as ''segmented trapezoidal PMs'', as shown in Fig. 1(d). As the number of segments is increased, the segmented trapezoidal PMs can be approximated to arbitrary PM shape, and achieve lower force ripple and greater average force for the LPMM. To determine the design parameter of segmented trapezoidal PMs, the multi-objective particle swarm optimization (PSO) is adopted in the optimal design process.

In this article, a double-sided LPPM for the kilometer-level electromagnetic launch system is presented. To enhance the average thrust force, reduce the thrust ripple and normal force of linear motor, a new PM shaping method is proposed, which can be called as ''segmented trapezoidal PMs''. The multi-objective PSO algorithm is adopted to balance the average thrust force and force ripple. Compared with the conventional PM shaping methods. the motors with 3-segmented trapezoidal PMs achieve lower force ripple, greater average force and lower manufacturing difficulty. The risk of PM demagnetization fault has been taken into account. To reduce the losses in the mover of the linear, a non-metallic light-weight mover structure is proposed. The rationality of segmented trapezoidal PMs and non-metallic light-weight are verified by the finite element method (FEM) and experiment.

II. LINEAR PERMANENT MAGNET MOTOR

A. BACKGOUND

The linear motor discussed in this paper is applied as the propulsion motor in a kilometer-level EMSL. The EMSL is designed to accelerate the objects to more than 800 km/h within 500 meters. The weight of accelerated object is 800kg. Thus, the rated thrust of the linear motor is 80 kN, and the weight of the mover is expected to be less than 250kg.

As a critical component in a complex system, the design of the propulsion motor is constrained by the other subsystem. For the high-power high-speed application, the pole pitch of the linear motor is constrained by the maximum current frequency of the inverter and the measurement accuracy of the position sensor. The maximum phase current and phase voltage are also constrained by the inverters.

When the velocity of the mover is more than 600 km/h, because of the coupling vibration, the contact support structure of the mover becomes unreliable. the magnetic levitation technology is applied in the high-speed linear motor. Thus, the additional guide device is necessary. Considering the control accuracy of the guide device, the high-speed linear motor always has a large air-gap. In summary, the design requirements and constraints are listed in the Table 1.

B. STRUCTRUE OF LPPM

For the kilometer-level EMLS, the long stators of the LPPM are fed segment by segment. Modular design is adopted for

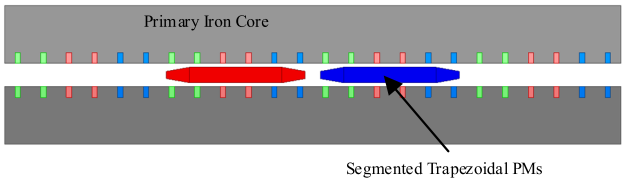

FIGURE 2. The structure of the LPPM with a stator section and a secondary.

the long-stator. The structure of the LPPM with a stator segment and a secondary is shown as Fig. 2.

The double-sided LPPM consists of two symmetrical primaries and a secondary with segmented trapezoidal PMs. The 3-phase windings are the full-pitch windings, which is located in the open slots.

C. SEGMENTED TRAPEZOIDAL PMS

The segmented trapezoidal PMs proposed in this paper consist of several trapezoidal PM segments. Segmentation is also an efficient method to reduce the eddy-current losses in PMs of high-power high-speed linear motors.

Without loss of generality, for n-segmented PM poles (n is odd), the height function of the PM pole can be expressed as

$$H_{pm}(x) = h_{pm}(i) + \left[h_{pm}(i+1) - h_{pm}(i)\right] \frac{2x - \prod_{k=1}^{i} k_a(i)\,\tau}{\prod_{k=1}^{i+1} k_a(i)\,\tau - \prod_{k=1}^{i} k_a(i)\,\tau}$$
$$x \in \left[-\frac{1}{2}\prod_{k=1}^{i} k_a(i)\,\tau, -\frac{1}{2}\prod_{k=1}^{i+1} k_a(i)\,\tau\right], i = 1, 2, \ldots, (n+1)/2 \tag{1}$$

Then, the dimension of the design variables is $n + 1$, and the design variables D_{opt} can be expressed as

$$D_{opt} = \left[h_{pm}(1), \ldots, h_{pm}\left(\frac{n+1}{2}\right), k_a(1), \ldots, k_a\left(\frac{n+1}{2}\right)\right] \tag{2}$$

The typical structures of segmented trapezoidal PMs are shown in Fig. 3. The pole is symmetrical about x-axial and y-axial. As an example, the design variables of the 3-segments trapezoidal PMs are $[h_{pm}(1), h_{pm}(2), k_a(1), k_a(2)]$, and τ is pole pitch of the motors. That is, the dimension of the optimal search space for 3-segments PM poles is 4. When $k_a(2)$=0, the motor with 3-segments PM poles is degenerated into the motor with 2-segments PM poles. In fact, any design variables have equivalent forms in the higher-dimension search space. It means that the better design variables also can be found in the motors with more PM segments.

D. COMPARATIVE ANALYSIS

As discussed above, the LPPM and LIM are two suitable topology structures for the kilometer-level high-speed EMLS.

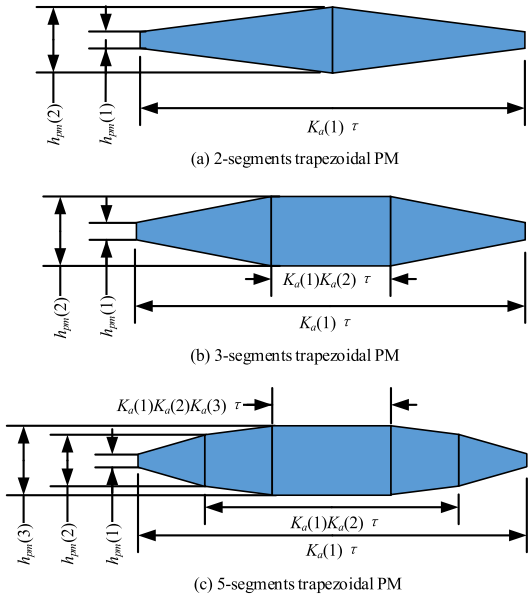

FIGURE 3. The structure of the segmented trapezoidal PMs. (a) 2-segments trapezoidal PM. (b) 3-segments trapezoidal PM. (c) 5-segments trapezoidal PMs.

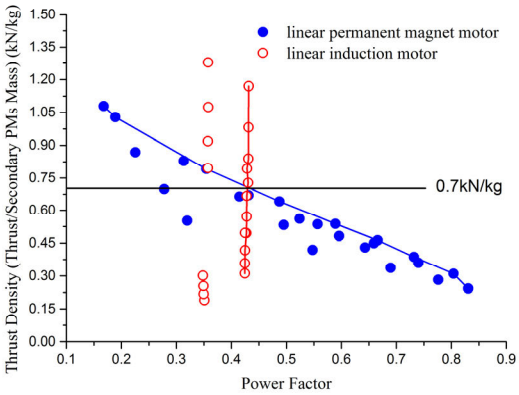

FIGURE 4. The main performances of the LPPM and LIM with different design parameters.

A simple comparative analysis between the LPPM and LIM is presented in this section.

Without loss of generality, the ratio of the primary pole number to the secondary is given as 2. Under design constrains listed in the Tab. 1, the main performances of the LPPM and LIM with different design parameters are shown in Fig. 4.

For the long-distance EMLS, the thrust density and power factor are two major performances of the linear motors. The thrust density is defined as the ratio of the average thrust force to the secondary PMs mass. As shown in Fig. 4, the LIM can achieve higher thrust density, and the LPPM has the advantage of high power factor when the thrust density of the LPPM is lower than 0.7kN/kg.

In practice, the stator segments are connected by the segment switches. Because of the high price of the segment

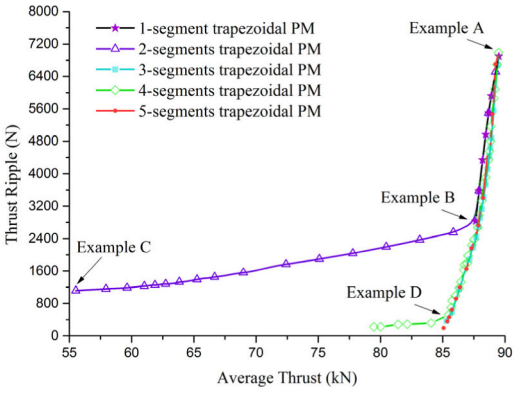

FIGURE 5. The Pareto front of the optimal design result.

switches, the segment switches become the major cost of the long-distance EMLS. Thus, under the voltage limit of the inverter, the LPPM has longer stator segments and less segment switches. It means that the LPPM has excellent cost advantage when the thrust density demand of the EMLS is relatively low.

III. PM OPTIMIZATION

A. OPTIMIZATION CONSTRAIN

To reduce the thrust ripple and enhance the average thrust force of the LPPM, a novel segmented trapezoidal PM shaping method is proposed in this paper. To clarify the effectiveness of the novel PM shaping method, the optimization analysis in this section focus on the segmented trapezoidal PMs. The basic design parameters of the LPPM are listed in the Tab. 2.

In practical, considered the support structure of PMs, the constrains about the design variables of segmented trapezoidal PM pole are shown as

$$h_{pm}(i) \in [0, 40] \text{ mm}$$
$$k_a(i) \in \begin{cases} (0, 1) & \text{if } i \neq 1 \\ (0, 0.95] & \text{if } i = 1 \end{cases} \quad (3)$$

To simplify the optimal process, the maximum height of the poles is determined as 40 mm, which means for n-segmented PM poles, the dimension of the design variables D_{opt} are n in the optimal design in this paper.

B. OPTIMIZATION ANALYSIS

The multi-objective PSO algorithm is adopted to reduce the thrust force and enhance the average thrust of the LPPM. The segmented trapezoidal PMs with different number of PM segments are analyzed by the 2-dimensional FEM. The Pareto front of the optimal design result is shown in Fig. 5.

1) 1-SEGMENT PM POLES

1-segment PM pole, or rectangle PM pole, has been widely applied in industry. Rectangle PM pole has only one design variable, k_{a1}. The Pareto front is a set of solution with variable k_{a1} belong to [0.86, 0.95].

When k_{a1} is 0.95 (Example A), the motor provides the maximum average thrust force. The average thrust force is 89.51 kN, and the force ripple is 6.89 kN. When k_{a1} is 0.86 (Example B), the motor achieves the minimum force ripple. The force ripple is reduced to 87.64 kN, while the average thrust force is reduced to 2.83 kN.

TABLE 2. Basic Design Parameters of LPPM.

Symbol	Items	Value
m	Phase number	3
p_{pri}	Primary poles number	12
p_{sec}	Secondary poles number	7
N_s	Slot number (Single side)	72
τ	Pole pitch	400 mm
h_{yoke}	Primary yoke thickness	125 mm
h_s	Height of slot	24.2 mm
W_s	Width of slot	12 mm
g	One-side air gap	10 mm
h_{pmmax}	PM maximum length	40 mm
L_{pri}	Primary stack height	270 mm
L_{pm}	PM height	235 mm
I	Phase current	6000 Arms

2) 2-SEGMENTS PM POLES

As shown in Fig. 5, when the average thrust force needs to be greater than 87.64 kN, 2-segments PM poles cannot provide better performance than rectangle PM poles.

On the other hand, compared with the rectangle PM poles, 2-segments PM poles can achieve lower force ripple, while the average thrust force demand is reduced further. In the design with minimum force ripple (Example C), the force ripple is 1.12 kN, while the average thrust force has been reduced to 55.52 kN. Obviously, it is useless to reduce the force ripple while the average force is reduced about 38%. The design variable of Example C is [0.93, 0.001, 0.04].

3) 3-SEGMENTS PM POLES

For any design variable to rectangle PM pole or 2-segments PM pole, there is better solutions to 3-segments PM pole. Several non-dominated solutions are listed in Table 3.

In the design with minimum force ripple (Example D), the force ripple is 0.37 kN, while the average thrust force has been reduced to 85.29 kN. Thus, the sacrifice of the average has been constrained in 5%. Compared with the 3-segments trapezoidal PMs, the benefit of the PM poles with more segments is non-significant. Therefore, the 3-segments trapezoidal PMs can meet the demands of most applications.

Previous studies have indicated that the high-order harmonics of magnetic field can be regarded as the main sources of the force ripple. Following this conclusion, the ideal magnetic field distribution is proposed in [15]. However, due to the leakage flux at the end of PMs, the ideal magnetic field

TABLE 3. Nondominated Solution of 3-Segmented PM Poles.

Design Parameters $[K_a(1), K_a(2), h_{pm}(1), h_{pm}(2)]$	Average Force (kN)	Force Ripple (kN)
(0.9500,0.5000,0.0400,0.0400)	89.51	6.89
(0.9492,0.8486,0.0303,0.0400)	89.08	5.56
(0.9492,0.7831,0.0310,0.0400)	88.90	4.88
(0.9499,0.7917,0.0261,0.0400)	88.59	4.11
(0.9496,0.7947,0.0203,0.0400)	88.26	3.38
(0.9325,0.7791,0.0208,0.0400)	87.78	2.59
(0.9233,0.7298,0.0207,0.0400)	87.03	1.83
(0.9146,0.7009,0.0184,0.0400)	86.15	0.97
(0.9017,0.6665,0.0187,0.0400)	85.29	0.37

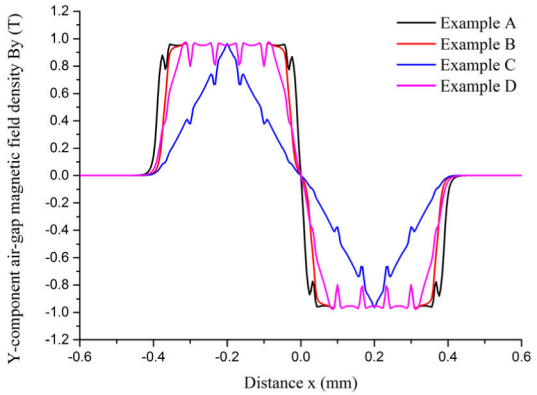

FIGURE 6. The Off-load air-gap magnetic field density distribution.

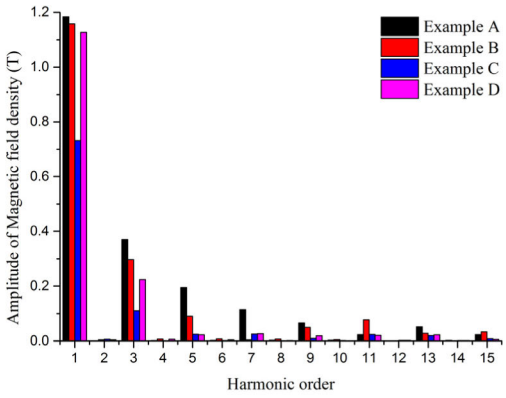

FIGURE 7. The harmonic distribution of the Off-load air-gap magnetic field density.

distribution cannot be obtained by the PM poles with the same height function.

The off-load air-gap magnetic field distribution is shown as Fig. 6, and their harmonic distribution are shown as Fig. 7. It shows that the average thrust force is proportional to the amplitude of the fundamental magnetic field density. For 3-phase motors, the 3-order harmonic magnetic field will not provide thrust force. But under the PM maximum height

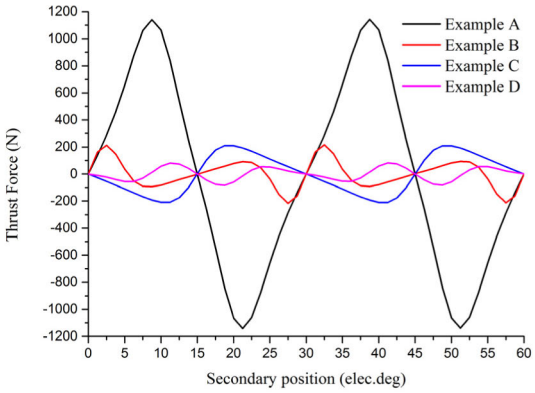

FIGURE 8. The off-load thrust force of the example A, B, C and D.

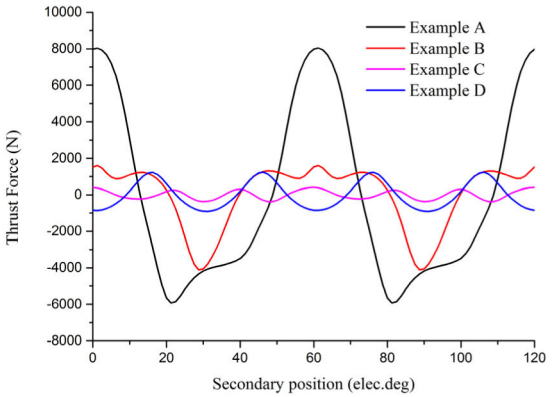

FIGURE 9. The on-load thrust force ripple of the example A, B, C and D (Without DC component).

constrain, the 3-order harmonic can enhance fundamental magnetic field, and then enhance the average thrust force. Although the high-order harmonics enhance the fundamental magnetic field, it also enhances the force ripple. Thus, the LPPM achieved greater average thrust and lower thrust ripple tend to remain the fundamental and 3-order harmonic magnetic field and reduce the higher-order harmonic magnetic field.

The off-load thrust force of the example A, B, C and D are shown as Fig. 8. The on-load thrust force ripple of the example A, B, C and D are shown as Fig. 9, and the on-load average thrust force of the motors is shown as Fig. 10.

The off-load thrust force is also called as 'detent force', which is caused by the slot and end effect. As shown in Fig. 8, when there is N_s slots in the single side of the motors with p_{pri} pole pairs primary, the frequency of the off-load thrust force is N_s/p_{pri} times as electrical frequency. For double-sided long primaries PMs linear motors, end effect cannot be the first cause. Due to slot effect, both fundamental PM magnetic field and harmonic magnetic field will lead to detent force. Thus, in the above 4 example s, the example A suffer from the maximum detent force (1.14 kN), while it provides the maximum fundamental magnetic field and amount of harmonic

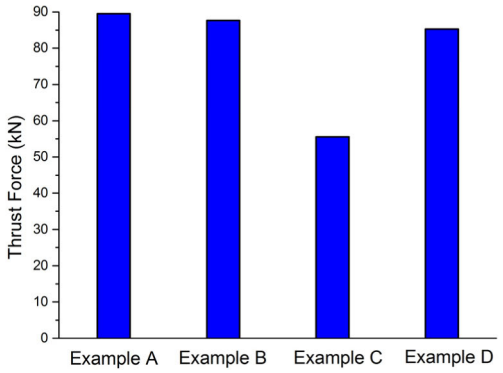

FIGURE 10. The on-load average thrust force of the example A, B, C and D.

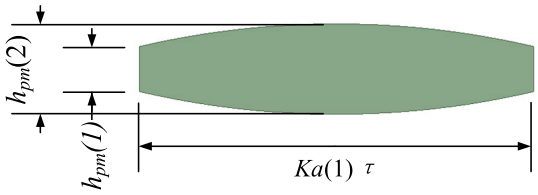

FIGURE 11. The design parameters of the eccentrically shaping PMs.

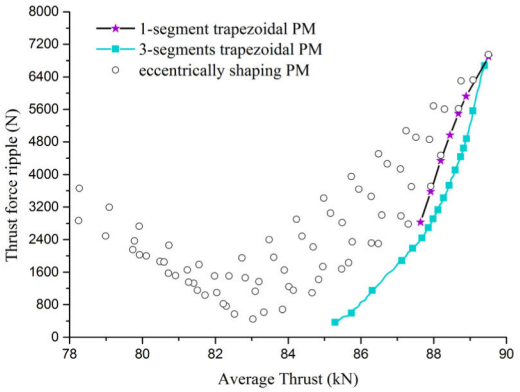

FIGURE 12. The thrust force characteristics of the LPPM with eccentrically shaping PMs.

TABLE 4. Nondominated Solution of 3-Segmented PM Poles.

	Average Force (kN)	Force Ripple (kN)	Maximum Normal Force (kN)
Example D	85.29	0.37	12.29
Example E	82.50	1.58	10.01

magnetic field. Although the PMs of the example A and B have the same height at the end of PMs, the example B has much less detent force (213 N). The example D has the minimum detent force (81 N), while it provides the less harmonic magnetic field than that of the example A and B. It seems that the harmonic magnetic field lead to detent force. However, the example C suffer from more detent force (209 N) than that of the example B, while the example C provide less fundamental and harmonic magnetic field.

As a high-power high-speed application, the double-sided long-primary PM linear motor always has fewer slot number and greater pole pitch. Thus, the armature magnetic field has significant harmonic component. As a results of the harmonic armature magnetic field, the on-load thrust force ripple is much greater than the detent force. Due to the optimal design of segmented trapezoidal PM pole, the on-load force ripple can be reduced to within the 0.5% of the average thrust force.

C. COMPARATIVE STUDY

The eccentrically shaping PM method is a popular PM shaping method. The structure parameters of the eccentrically shaping PMs are shown in Fig. 11. The design parameters of eccentrically shaping PMs are determined by parameter sweep method.

The thrust force characteristics of the LPMM with eccentrically shaping PM is shown in Fig. 12. As shown in the Fig. 12, the minimum thrust force of LPPM with eccentrically shaping method is 448 N, while the average thrust force is 83.03kN. Thus, the LPPM with 3-sgemented trapezoidal PMs can achieved less force ripple while the average thrust can be increased by 2.7% than that of the LPPM with eccentrically shaping PMs. Furthermore, the segmented trapezoidal PMs has the advantages of lower manufacturing difficulty and lower cost.

D. NORMAL FORCE ANALYSIS

In practice, more electromagnetic performances have to be taken into account. Compared with the single-side LPPM, the double-sided LPPM has the advantages of low normal force on its mover. When the mover is located in the center of the double-sided stators, the normal force on the mover is zero. However, when the mover offset to the normal positive direction, the electromagnetic attraction force between the mover and double-sided stators become unbalance, and the resultant force make the mover away from the center of the LPPM. For the LPPM adopted magnetic levitation technology, the offset normal force on the mover is a main design parameter of the additional guide device in the high-speed EMLS.

Under the constraint of the output power and control accuracy of the guide device, the maximum deviation of the mover in normal direction is limited to 3 mm, and the maximum offset normal force of the mover is limited to 10 kN. Consider the above constraints, the design parameters of the 3-segments PMs have been further optimized. The Pareto front of the optimal design considered the offset normal force is shown as Fig. 13. Finally, the example E has been proposed. The design parameters of the 3-segments trapezoidal PMs in the example E are [0.8875, 0.5877, 0.015,0.04]. The main performances of the example D and example E are listed in Table 4. To reduce the maximum normal force on the mover, the average force and force ripple have been sacrificed in varying degrees.

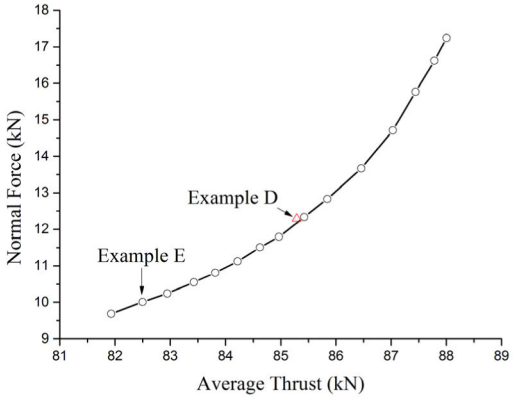

FIGURE 13. The Pareto front of optimal design considered the offset normal force.

TABLE 5. The Demagnetization Curve Knee Point of N52H and N48SH.

	Demagnetization curve knee point (T)	
Temperature (°C)	N52H	N48SH
30	-0.25	-0.57
60	0.07	-0.25
80	0.21	-0.02
100	0.41	0.22

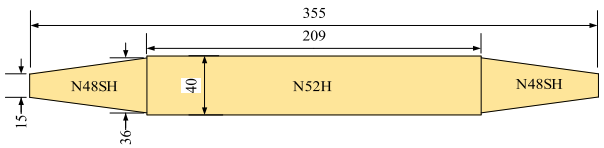

FIGURE 14. The design scheme of the segmented trapezoidal PM pole in the proposed LPPM.

E. RISK ANALYSIS OF DEMAGNETIZATION FAULT

The demagnetization fault is a common fault for the LPPM, which has to be analyzed in the design stage. When the PM shaping method is adopted, the end height of the PM poles are decreased, and the operating point of the PMs are decreased. Thus, the shaped PM poles have greater risk of demagnetization fault.

To reduce the risk of demagnetization fault, two different NdFeB materials (N52H and N48SH) are applied in the proposed segmented trapezoidal PMs. The remanence of the N52H NdFeB magnet is 1.42T, and the remanence of the N48SH NdFeB magnet is 1.37T. The demagnetization curve knee point of the N52H and N48SH are listed in Table 5. Because the N52H has greater remanence and N48SH has better heat resistance. The main part of the segmented trapezoidal PMs in the high-power LPPM can adopt N52H magnet, and the N48SH magnet is adopted at the ends of the PM pole. Based on the example E, the final design scheme of the segmented trapezoidal PMs in the proposed LPPM is shown in the Fig. 14.

The on-load magnetic field distribution in the centre of the PM is shown as Fig. 15. As shown in Fig. 14, the minimum operating point of the PM is -0.25 T. Thus, by using N48SH instead of N52H, the maximum operating temperature increases from 30 °C to 60 °C.

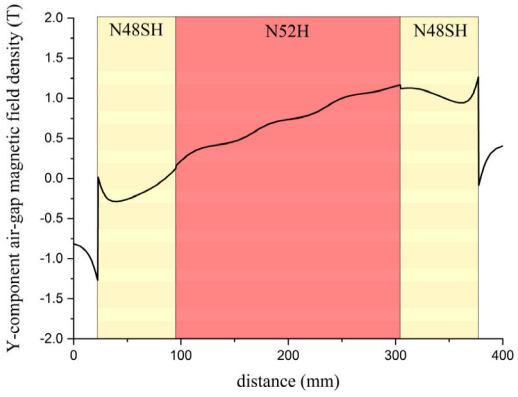

FIGURE 15. The on-load air-gap magnetic field density in the centre of the PM.

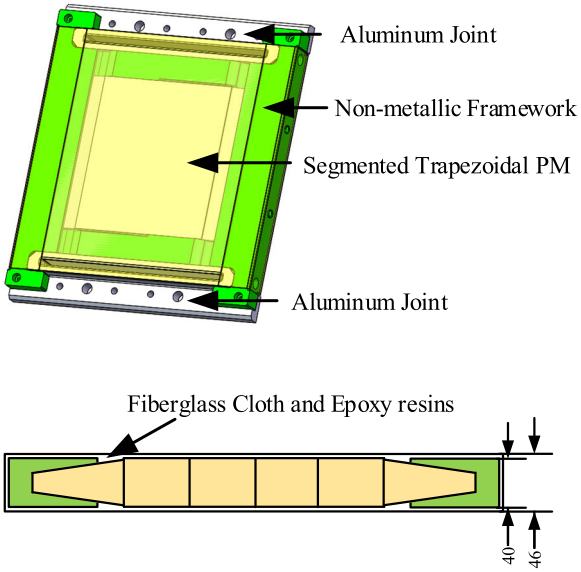

FIGURE 16. The non-metallic light-weight mover structure.

F. NON-METALLIC LIGHT-WEIGHT MOVER STRUCTURE

To avoid the eddy current loss in the metallic part of the mover and reduce the weight of the mover, a novel non-metallic light-weight mover structure is proposed in this paper, as shown in Fig. 16.

To reduce eddy current loss, the PMs have been segmented further. The PM segments are fixed by adhesives first and located in the non-metallic framework. Then, the PMs and framework are covered by fiberglass cloth and epoxy resins.

IV. EXPERIMENT

To validate the effectiveness of the proposed double-sided LPPM with segmented trapezoidal PMs, a experimental prototype has been manufactured, as shown in Fig. 17. The prototype consists of a single-segment double-sided stators and a secondary with a single-pole PM. The design parameters of the LPPM are the same as the parameter listed in the Table 2 but the pole number of the secondary. The structure of the segment trapezoidal PM is shown as Fig. 14. The weight of the mover is 36 kg.

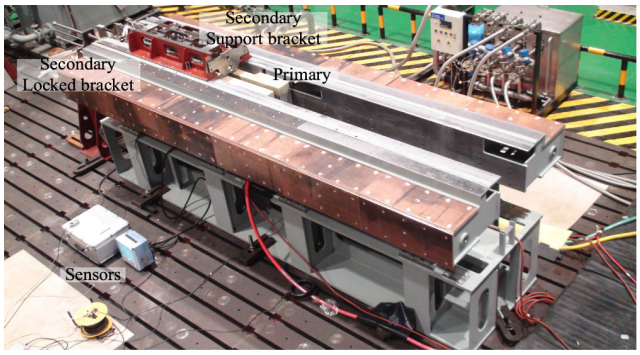

FIGURE 17. The double-sided LPPM with segmented trapezoidal PMs.

TABLE 6. The Inductance Matrix of The LPPM.

Symbol	2D FEM result	3D FEM result	Experimental result
L_{aa} (uH)	107.82	157.93	168.64
L_{ab} (uH)	-31.65	-35.12	-31.04
L_{ac} (uH)	-38.82	-56.41	-61.42

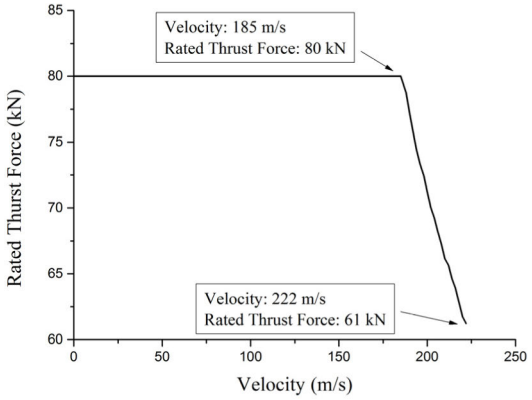

FIGURE 18. The characteristics curve of the rated thrust force and the velocity of the mover.

The off-load tests and locked-secondary have been done in this paper. In the off-load tests, the secondary of the motor has been taken down, and the armature windings are excited by the rated current. Based on the waveform of the 3-phase current and voltage, the inductance matrix of 3-phase windings can be calculated, which is listed in Table 6. The leakage inductance of ends of stator windings has been ignored in the 2D FEM, which lead to the difference between the result from the 2D FEM and 3D FEM.

Based on the performances measured in the off-load tests, the dynamic performance of the proposed LPPM has been simulated. Under the limit of the maximum output voltage, the characteristics curve of the rated thrust force and the speed of the LPPM is shown as Fig. 18. Considering the aerodynamic resistance force, the double-sided LPPM meet the design requirements.

In the locked-secondary tests, the secondary of the motor has been locked, and the armature windings are excited by the direct current, following the strategy about Id=0. The thrust force has been measured when the secondary is locked at different relative position. The result of the locked-secondary

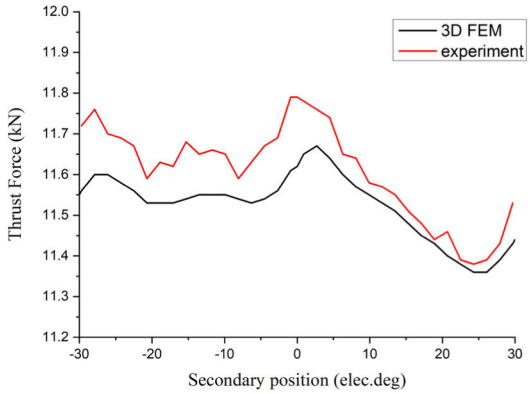

FIGURE 19. The thrust force measured in the experiment.

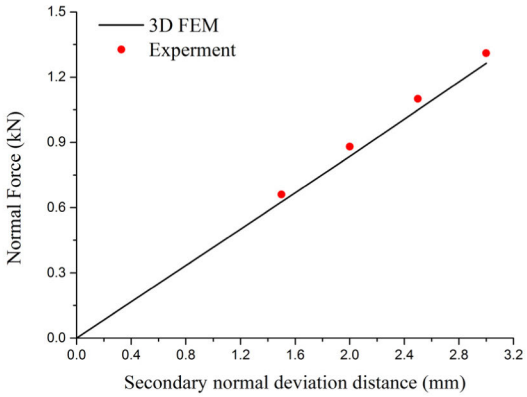

FIGURE 20. The relationship between the normal force and secondary normal deviation distance.

tests are shown in the Fig. 19. According to the experimental result, the average thrust force is 11.61kN, the thrust force ripple is 1.84% of the average thrust force.

The no-load normal force of the mover has been measured in the locked-secondary tests. For the mover with a single-pole PM, the relationship between the normal force and secondary normal deviation distance is shown in the Fig. 20. When the normal deviation distance is 3 mm, the normal force is measured as 1.31kN, while the result of the 3D FEM is 1.26kN.

The double-sided LPPM meet the design requirements. The experimental result verify the result from the FEM. The effectiveness of the conclusions about the double-sided LPPM with novel segmented trapezoidal PMs and non-metallic light-weight mover has been verified.

V. CONCLUSION

In this paper, a double-sided LPPM is presented for the high-speed kilometer-level EMLS. The target of the EMLS is to accelerate the object to more than 800 km/h in 500 meters and stop the object in another 500 meters. the rated thrust of the linear motor is 80 kN, and the weight of the mover is expected to be less than 250kg. Compared with the LIM, the double-sided LPPM has cost advantage when the thrust density demand of the EMLS is relatively low.

To enhance the average thrust force, reduce the thrust ripple and normal force of linear motor, a new PM shaping method is proposed, which can be called as ''segmented trapezoidal PMs''. The segmented trapezoidal PMs with different number of PM segments are analyzed. Compared with the motors providing the maximum average thrust force, the force ripple of the motors with 3-segmented PM poles can be reduced 94.6% at most while the average thrust force is reduced 4.7%. And compared with the traditional eccentrically shaping PMs, the motors with 3-segmented trapezoidal PMs achieve less force ripple, greater average force, lower manufacturing difficulty and lower cost. Thus, the motors with 3-segmented PM poles can meet the most requirements after optimization.

In practice, the normal force and the risk of demagnetization fault have been taken into account. to avoid the eddy current loss in the metallic part of the mover and reduce the weight of the mover, a novel non-metallic light-weight mover structure is proposed.

To validate the effectiveness of the proposed double-sided LPPM with segmented trapezoidal PMs, a experimental prototype has been manufactured. The experimental result verify the result from the FEM. The effectiveness of the conclusions about the double-sided LPPM with novel segmented trapezoidal PMs and non-metallic light-weight mover has been verified. The double-sided LPPM presented in this paper meet the design requirements.

REFERENCES

[1] H. D. Fair, ''The science and technology of electric launch,'' *IEEE Trans. Magn.*, vol. 37, no. 1, pp. 25–32, Jan. 2001, doi: 10.1109/20.911783.

[2] H. D. Fair, ''Electromagnetic launch science and technology in the united states enters a new era,'' *IEEE Trans. Magn.*, vol. 41, no. 1, pp. 158–164, Jan. 2005, doi: 10.1109/TMAG.2004.838744.

[3] D. Patterson, A. Monti, C. W. Brice, R. A. Dougal, R. O. Pettus, S. Dhulipala, D. C. Kovuri, and T. Bertoncelli, ''Design and simulation of a permanent-magnet electromagnetic aircraft launcher,'' *IEEE Trans. Ind. Appl.*, vol. 41, no. 2, pp. 566–575, Apr. 2005, doi: 10.1109/TIA.2005.844404.

[4] L. Li, M. Ma, B. Kou, and Q. Chen, ''Analysis and design of moving-magnet-type linear synchronous motor for electromagnetic launch system,'' *IEEE Trans. Plasma Sci.*, vol. 39, no. 1, pp. 121–126, Jan. 2011, doi: 10.1109/TPS.2010.2053722.

[5] K. Bao-Quan, W. Hong-Xing, L. Li-Yi, Z. Liang-Liang, Z. Zhe, and C. Hai-Chuan, ''The thrust characteristics investigation of double-side plate permanent magnet linear synchronous motor for EML,'' *IEEE Trans. Magn.*, vol. 45, no. 1, pp. 501–505, Jan. 2009, doi: 10.1109/TMAG.2008.2008887.

[6] N. R. Tavana, A. Shoulaie, and V. Dinavahi, ''Analytical modeling and design optimization of linear synchronous motor with stair-step-shaped magnetic poles for electromagnetic launch applications,'' *IEEE Trans. Plasma Sci.*, vol. 40, no. 2, pp. 519–527, Feb. 2012, doi: 10.1109/TPS.2011.2178616.

[7] R. Cao, Y. Jin, Z. Zhang, and M. Cheng, ''A new double-sided linear flux-switching permanent magnet motor with yokeless mover for electromagnetic launch system,'' *IEEE Trans. Energy Convers.*, vol. 34, no. 2, pp. 680–690, Jun. 2019, doi: 10.1109/TEC.2018.2867625.

[8] W. Zhao, J. Zheng, J. Wang, G. Liu, J. Zhao, and Z. Fang, ''Design and analysis of a linear permanent-magnet Vernier machine with improved force density,'' *IEEE Trans. Ind. Electron.*, vol. 63, no. 4, pp. 2072–2082, Apr. 2016, doi: 10.1109/tie.2015.2499165.

[9] R. Cao, M. Lu, N. Jiang, and M. Cheng, ''Comparison between linear induction motor and linear flux-switching permanent-magnet motor for railway transportation,'' *IEEE Trans. Ind. Electron.*, vol. 66, no. 12, pp. 9394–9405, Dec. 2019, doi: 10.1109/tie.2019.2892676.

[10] M. Mirzaei, S. E. Abdollahi, and H. Lesani, ''A large linear interior permanent magnet motor for electromagnetic launcher,'' *IEEE Trans. Plasma Sci.*, vol. 39, no. 6, pp. 1566–1570, Jun. 2011, doi: 10.1109/tps.2011.2140401.

[11] M. Ma, L. Li, Z. He, and C. C. Chan, ''Influence of longitudinal end-effects on electromagnetic performance of a permanent magnet slotless linear launcher,'' *IEEE Trans. Plasma Sci.*, vol. 41, no. 5, pp. 1161–1166, May 2013, doi: 10.1109/tps.2013.2250523.

[12] Y. Li, J. Xing, T. Wang, and Y. Lu, ''Programmable design of magnet shape for permanent-magnet synchronous motors with sinusoidal back EMF waveforms,'' *IEEE Trans. Magn.*, vol. 44, no. 9, pp. 2163–2167, Sep. 2008, doi: 10.1109/TMAG.2008.2000750.

[13] K. Wang, Z. Q. Zhu, and G. Ombach, ''Torque enhancement of surface-mounted permanent magnet machine using third-order harmonic,'' *IEEE Trans. Magn.*, vol. 50, no. 3, pp. 104–113, Mar. 2014, doi: 10.1109/TMAG.2013.2286780.

[14] F. Chai, P. Liang, Y. Pei, and S. Cheng, ''Magnet shape optimization of surface-mounted permanent-magnet motors to reduce harmonic iron losses,'' *IEEE Trans. Magn.*, vol. 52, no. 7, Jul. 2016, Art. no. 6301304, doi: 10.1109/TMAG.2016.2524010.

[15] N. Roshandel Tavana and A. Shoulaie, ''Analysis and design of magnetic pole shape in linear permanent-magnet machine,'' *IEEE Trans. Magn.*, vol. 46, no. 4, pp. 1000–1006, Apr. 2010, doi: 10.1109/TMAG.2009.2037951.

[16] Y. Li, J. Zou, and Y. Lu, ''Optimum design of magnet shape in permanent-magnet synchronous motors,'' *IEEE Trans. Magn.*, vol. 39, no. 6, pp. 3523–3526, Nov. 2003, doi: 10.1109/TMAG.2003.819462.

[17] A. H. Isfahani, ''Analytical framework for thrust enhancement in permanent-magnet (PM) linear synchronous motors with segmented PM poles,'' *IEEE Trans. Magn.*, vol. 46, no. 4, pp. 1116–1122, Apr. 2010, doi: 10.1109/TMAG.2009.2036993.

[18] Y. Shen and Z. Q. Zhu, ''Investigation of permanent magnet brushless machines having unequal-magnet height pole,'' *IEEE Trans. Magn.*, vol. 48, no. 12, pp. 4815–4830, Dec. 2012, doi: 10.1109/TMAG.2012.2202398.

[19] Y. Zhang, Z. Yang, M. Yu, K. Lu, Y. Ye, and X. Liu, ''Analysis and design of double-sided air core linear servo motor with trapezoidal permanent magnets,'' *IEEE Trans. Magn.*, vol. 47, no. 10, pp. 3236–3239, Oct. 2011, doi: 10.1109/TMAG.2011.2156398.

DUNHUANG XU is currently pursuing the Ph.D. degree in electrical engineering with the Naval University of Engineering, Wuhan. His current research interest includes linear motor design.

DONG WANG received the Ph.D. degree in electrical engineering from the Naval University of Engineering, Wuhan, in 2007. He is currently a Professor and a Supervisor of Ph.D. candidates with the Naval University of Engineering. His current research interests include electric propulsion and integrated power generation systems.

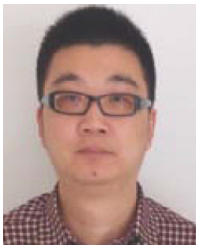

MING YAN received the Ph.D. degree in electrical engineering from the Naval University of Engineering, Wuhan, in 2015. He is currently an Associate Professor with the Naval University of Engineering. His current research interest includes motor design and analysis.